Tikhonov's regularization for deconvolution in the empirical Green function method and vertical directivity effect

N. Kraeva*

Institute of Marine Geology and Geophysics, Far East Branch of Russian Academy of Sciences, Nauki Street, 1b, Yuzhno-Sakhalinsk 693022, Russia

Abstract

Application of Tikhonov's technique, using input errors for the parameter of regularization estimation, enhances the accuracy and stability of the reconstruction of a source time function (STF) by the empirical Green function (EGF) method that gives us an opportunity to use simultaneously for analysis body and surface waves data, and to estimate the horizontal and vertical directivity effects. Knowledge of the last is particularly useful for the choice of an active nodal plane of earthquakes with the dip slip fault orientation that allows us to classify these earthquakes to the interplate or intraplate types and thereby to reach the better understanding of tectonic processes in the region of interest.

By way of illustration, an attempt to estimate average parameters of faulting in a first approximation is made herein for two Russian Far East large events with opposite types of focal mechanism orientation, strike slip and dip slip. The former is not a matter of interest in the context of vertical directivity effect but enables us to test the method.

The directivity analysis of pulse durations and inverse amplitudes of the relative source time functions (RSTFs) restored at eight globally distributed stations IRIS indicates that the destruction in the source of the Neftegorsk earthquake (05/27/1995 $M_W = 7.1$) propagated roughly horizontally in the direction $8 \pm 11°$ during 19.2 ± 0.4 s along the rupture extending 35.5 ± 4.9 km. The calculated slip distribution along the rupture coincides within the error with the results of field geological measurements on the causal surface fault that proves that the Neftegorsk earthquake source is well described by the model of the linear unilateral fault and gives a good assessment of the method applied.

The average parameters of faulting in the Kamchatka earthquake (03/08/1999 $M_W = 6.9$) have been determined from data of 13 station IRIS. It was shown that the destruction in its source propagated downward at an angle of about $60°$ with horizon, in the direction about S156° E, during 13.4 ± 0.2 s, along the rupture totaling 25.5 ± 2.3 km in length. Therefore, the nodal plane, steeply dipped to the SE, was active and this event can be regarded as an intraplate type. Two asperities can be selected; the first with the maximum slip 3.3 m located at a distance of about 7 km from the onset of rupture, and the second with the maximum slip about 0.9 m centered at approximately 19 km from that.

© 2004 Elsevier B.V. All rights reserved.

Keywords: Filtration of irregular solutions; Relative source time function; Fault slip distribution; Intraplate and interplate types

* Fax: +7-4242-791-517.
E-mail addresses: NKraeva2002@yandex.ru, Kraeva@imgg.ptcom.ru (N. Kraeva).

1. Introduction

How in the point of observation can a source time function (STF) be reconstructed? The main puzzle in this problem is the separation of the path and source effects. There are two approaches to its solution— deterministic and semiempirical. The first one has a limited application because of the impossibility of estimating all the different scale medium heterogeneities in a calculation of the impulse response of the propagation channel. Hence, only the simplest models of medium can be used, like homogeneous half space (e.g., Ruff and Kanamori, 1983; Beck and Ruff, 1984) and therefore all discounted path features are included in the source effect estimation.

The second approach offered in Hartzell (1978) and named empirical Green function (EGF) method is used more and more frequently with digital seismological networks and hardware development. The main idea of this method is to let the Earth itself calibrate the propagation effects, and to consider as an impulse response of the given propagation channel the seismogram of the weaker event from the same region and with the same focal mechanism as the earthquake of interest. This allows us to avoid the need to calculate theoretical seismograms for complex mediums and simplifies greatly the problem of STF extraction, reducing it to the solution of the problem of deconvolution of one seismogram from another.

The set of the restored relative STFs with azimuthal and takeoff angle variations provides a way of studying the finiteness of the event and estimating, within the scope of the line unilateral source model, a slip distribution along the rupture, and also of retrieving a direction of the main "strike attack" of the earthquake and its average rupture length, duration and velocity. This analysis is performed for small events using short-period body waves recorded by local seismic networks (e.g., Mueller, 1985; Li and Thurber, 1988; Mori, 1996 and others) and for moderate-sized and large earthquakes using teleseismic and regional broadband records of body or surface waves recorded by the global seismological network (e.g., Ruff and Kanamori, 1983; Beck and Ruff, 1984; Schwartz and Ruff, 1985; Ammon et al., 1993; Velasco et al., 1994a,b; Cassidy, 1995 and many others). The simplicity of the method makes it possible to use it in regional seismological centers as an alternative method for quick determination of the generating fault and identification of the strongest destruction region, thereby helping to coordinate rescue teams (Ammon et al., 1993; Velasco et al., 1994b).

In this work, the routine approach in a space– time rupture process research is updated by two elements. First, for the solution of the ill-posed deconvolution problem, it does not used the traditional "water level" or similar white noise damping (Owens et al., 1984; Mueller, 1985; Li and Thurber, 1988; Mori and Frankel, 1990; Sherbaum and Johnson, 1994; Ammon et al., 1993; Velasco et al., 1994a,b; Cassidy, 1995; Hough and Dreger, 1995; Mori, 1996) or damped least-squares method (Sipkin and Lerner-Lam, 1992; Gurrola et al., 1995) but Tikhonov's regularization technique (Tikhonov and Arsenin, 1977; Tikhonov et al., 1995) ensuring the stability and accuracy of the solution. And second, based on the set of stable determined relative STFs, an attempt is made to detect and estimate, albeit roughly, a vertical directivity effect (Lay and Wallace, 1995) which in the case of an earthquake with near dip slip focal mechanism helps to choose unambiguously an active nodal plane. In this work, the algorithm of the linear source dip angle determination is a part of the directivity analysis applied simultaneously to body and surface waves data.

2. Method

The EGF method operates with a pair of earthquakes. The main, which is the subject of our interest, and the auxiliary, which is the weaker event from the same region, with the same focal mechanism as the main. Let us mark the far-field displacement wavelet, which is an isolated phase with an inherent ray parameter, of the main and auxiliary events as $u(t)$ and $g(t)$, respectively. Then, following (Hartzell, 1978; Mueller, 1985; Zollo et al., 1995), with a large enough difference between the magnitudes of these events, the desired relative source time function (RSTF), $z(t)$, normalized to the auxiliary event seismic moment M_g, can be found by the deconvolution in the frequency domain of the auxiliary event waveform from that of the main event with the following low pass filtering of the result with a

cutoff frequency equal to the corner frequency of the auxiliary event, f_c^g:

$$\tilde{z}(f) = \frac{\tilde{u}(f)}{\tilde{g}(f)} \text{ for } f < f_c^g, \tag{1}$$

where $\tilde{u}(f)$, $\tilde{g}(f)$ and $\tilde{z}(f)$ represent the spectra of the large event, smaller event and normalized RSTF, respectively. This equation is based on the assumption of linearity of the system source seismometer and the source mechanism being kept constant during the main event source process.

There are rather strict constraints imposed on the auxiliary earthquake. Namely, its magnitude must be below the one of the main earthquake by not less than one unit, hypocenter depths must differ no more than 20 km, and epicenters must be at a distance from each other of not more than two fault lengths of the main earthquake (Velasco et al., 1994a,b). The degree of coincidence of the focal mechanisms remains an open question. It is clear that this consilience must be as exact as possible.

It is also obvious that the method should be used with caution for very strong earthquakes, the RSTFs of which can be so long that the isolation of different phases on many seismograms can prove to be impossible. Besides, the focal mechanisms of such sources can vary greatly during their source process.

The problem of deconvolution [Eq. (1)] pertains to the class of ill-conditioned problems. In general, all methods of their solution are reduced on physical essence to the filtration of irregular solutions, and the main task is to choose the optimal degree of this filtration. Let us consider Tikhonov's method of regularization (Tikhonov and Arsenin, 1977; Tikhonov et al., 1995) and show that it gives an objective way of this optimal degree finding.

The problem of ill condition in this technique is overcome by means of Tikhonov's stabilizer, of which kind depends on the choice of the solution metric space. The optimal choice for the digital seismogram processing is obviously the Hilbert space, in which a vicinity of functions is considered as the vicinity on an average, and a convergence is root mean square. In the Hilbert spaces, Tikhonov's stabilizer in the problem of deconvolution without limitations is simply the norm of its solution.

In view of we want to restore RSTFs in as much details as possible, searching for the solution is produced in the space L_2 of square integrable functions. This means that the solution converges to the desired one root-mean-squarely (separate outliers are possible) and decreases with growing of frequency not slower, than $f^{-\frac{1}{2}}$. Notice that input digital data belongs to the same space. In this case the solution of the problem of deconvolution of the EGF, $g_h(t)$, from the main event waveform, $u_\delta(t)$ is equal to the convolution:

$$z_\eta^\alpha(t) = u_\delta(t) * K_h^\alpha(t). \tag{2}$$

The conversion kernel here has the following form:

$$K_h^\alpha(t) = \int_{-\infty}^{+\infty} \frac{1}{\tilde{g}_h(f)} \cdot \frac{|\tilde{g}_h(f)|^2}{|\tilde{g}_h(f)|^2 + \alpha} \cdot \exp(j2\pi ft)\mathrm{d}f, \tag{3}$$

where α is the parameter of regularization and $\eta = (\delta, h)$ is a pair of values, characterizing an inaccuracy of the input data: $\|u_\delta(t) - \bar{u}(t)\|_{L_2} \leq \delta$ and $\|A - A_h\|_{L_2 \to L_2} \leq h$. Here $\bar{u}(t)$ and A are the exact meanings of the main event seismogram and the convolution operator imaging the metric space of RSTFs into the metric space of input waveforms, $u_\delta(t)$ and A_h are their real meanings with noise.

The conversion kernel [Eq. (3)] coincides with that of the damped least-squares deconvolution (Sipkin and Lerner-Lam, 1992; Gurrola et al., 1995). The essential difference between these two deconvolution techniques lies in the manner of finding an optimal value of the regularization parameter α. Tikhonov's method matches it with the input data error so that the solution misfit would be equal to this error:

$$\|g_h * z_\eta^\alpha - u_\delta\| = (\delta + h\|z_\eta^\alpha\|). \tag{4}$$

The root of this equation is determined iteratively. It is proven in Tikhonov et al. (1995) that the approximate solution $z_\eta^\alpha(t)$ found for optimal α is single and tends at decreasing of the input data error root mean squarely to the exact one. In contrast, at the damped least-squares deconvolution, the value of α is estimated subjectively on the speed of the decrease of the solution misfit at $\alpha \to 0$ (Gurrola et al., 1995) which is in the case in point strictly monotonous on α (Tikhonov et al., 1995) so that the found solution is quasioptimal (Tikhonov et al., 1979).

Tikhonov's regularization technique takes into account both numerator and denominator inaccuracies in Eq. (1). They can be estimated from the preevent microseism noise. It can be shown that the error of the main event waveform is about $\delta \approx \sigma_u^{\mathrm{ms}} \sqrt{T_u}$, where σ_u^{ms} is standard deviation of the microseism background on which the input data $u_\delta(t)$ was registered, T_u is the time interval of this input row in seconds. The estimation of the convolution operator error h turns out to be more complex and demands an iterative procedure (Kraeva, 2001). As its zero upper estimation we can take $h_0 = \sigma_g^{\mathrm{ms}} \sqrt{T_g T_u}$, where σ_g^{ms} is the standard deviation of the microseism background $a_g^{\mathrm{ms}}(t)$ on which the auxiliary earthquake was registered, T_g is the length of its record in seconds. Using solution z got at $h = h_0$ we can find a more accurate estimation of this error $h \approx \| a_g^{\mathrm{ms}}*z \| / \| z \|$. The procedure is repeated several times unless the value h stabilizes.

If to compare Tikhonov's regularization algorithm with the most frequently used for the RSTF reconstruction spectral division with "water level" correction (Sherbaum and Johnson, 1994; Sherbaum, 1996), the advantage of the former is evident. Tikhonov's algorithm, using input errors for the parameter α calculation, allows us to give a real and stable estimation of STF readily, while in the case of "water level" we always have to choose the regularization parameter by intuitively and to try several solutions. What is more, an incorrect guess results in a mistake in the shape and amplitude of the restored STF.

Because a seismic signal spectrum decays when frequency grows, the second multiplier in the conversion kernel [Eq. (3)] is the low pass filter. Its cutoff frequency depends on the value of input data noise contamination. The larger the noise, the smaller this frequency becomes and the stronger the smoothing. Thus, as a result of the solution of the deconvolution problem by means of Tikhonov's algorithm at a number of stations, we get the set of n RSTFs, smoothed to various degrees. Analyzing a signal/noise (S/N) ratio on the records of the EGFs as a function of frequency, we can determine corresponding resolution frequencies $f^{\mathrm{S/N}}$ as those when this ratio begins to exceed 2. The minimum from frequencies $f_c^g, f_i^{\mathrm{S/N}}$, $i = 1, \ldots, n$, is then chosen as the cutoff frequency of the resulting low pass filter. This filtering cuts off high-frequency information connected with the source finiteness effects of the auxiliary event, and simultaneously makes all restored RSTFs comparable with each other on the smoothing degree (Kraeva, 2001, 2003).

3. Digital data analysis

In this study, digital long period seismograms recorded by 16 IRIS stations were used for the reconstruction of RSTFs. At present, the global network GSN has enough density to provide us with the minimal amount of records only of the auxiliary events with magnitudes $M > 5 - 5.5$. The corner frequency of P-wave displacement spectra of such events is usually equal to 0.2 Hz or less. Thereby, the work range of periods is $T \geq 5$ s, and the discretization frequency 1 sample per s of the long period channel LP is sufficient for application of the discussed method to waveforms of earthquakes of such power.

The level of noise contaminating the auxiliary earthquake record is determinative for the feasibility of the corresponding RSTF reconstruction. It strongly depends on the frequency interval of the observations (Kraeva, 1996). Within the range of periods, $1 - 8$ s, there is the peak of "storm" microseisms. These sorts of microseisms, being somehow or other present at all LP channel records, are used for estimation of the input data error. The expected RSTF duration of the earthquakes with $M = 6.5 - 7.5$ is $10 - 50$ s that falls into the range of the microseism local minimum. The noise with longer periods does not give too many problems since restored RSTFs are visualized on the background of this noise reliably enough.

4. Source model

To interpret the restored RSTFs, the model of the linear unilateral fault of length L rupturing at constant velocity V_{R} is used herein. This model is the special case of Haskell's (1964) model, when the data resolving ability is sufficient for estimation of the source spatial variations only along a single coordinate axis. The far-field time function of the linear source has the finite width equal to (e.g., Lay and Wallace, 1995)

$$T_{\mathrm{R}} = T_0 - L \cdot \Gamma, \tag{5}$$

where $T_0 = L/V_R$ is the rupture duration, $\Gamma = \cos\theta/c$ is the directivity parameter, c is the phase velocity of the given wave in the vicinity of the source, θ is the angle between the ray leaving the source into the point of observation and the rupture direction. Thus, the width of the pulse T_R radiated in the process of the rupture propagation must change depending on the value of the parameter Γ.

Expressing the direction cosine, $\cos\theta$, as a scalar product of unit vectors directed along the rupture and outgoing ray, we can find

$$\cos\theta = \sin i_0 \sin i_h \cos(\alpha - \alpha_0) + \cos i_0 \cos i_h. \qquad (6)$$

Here i_0 is the linear source dip angle measured from the positive direction of the axis z (downwards) to the rupture direction ($0° \leq i_0 \leq 180°$), α_0 is the rupture direction azimuth, i_h is the takeoff angle of the given emitted wavelet, measured from the downward vertical axis ($0° \leq i_h \leq 90°$ for P, S and surface waves), α is the station azimuth.

Substituting Eq. (6) into Eq. (5) yields

$$T_R = T_0 - L_{hor}p_{hor}\cos(\alpha - \alpha_0) - L_{ver}p_{ver}, \qquad (7)$$

where $L_{hor} = L\sin i_0$ and $L_{ver} = L\cos i_0$ are the horizontal and vertical projections of the fault length, $p_{hor} = \sin i_h/c$ and $p_{ver} = \cos i_h/c$ are the inverse apparent velocities along the surface and vertical, respectively. It follows from this equation that the source finiteness has the horizontal and vertical components and the effect of vertical directivity can be detected only from body wave data because for surface waves the takeoff angle $i_h = 90°$ and $p_{ver} = 0$.

The correlating least-square analysis of linear Eq. (5) for a set of measured durations $T_R^i(\Gamma_i)$ of RSTFs deconvolved from body waves at several stations surrounding the epicenter, allows us to calculate the pair of angles (α_0, i_0) defining the rupture direction in horizontal and vertical planes, as well as the rupture duration $T_0 = L/V_R$ and length L. In the case of only surface waves data, we can retrieve only the two-dimensional horizontal picture of the rupture process: the azimuth α_0, duration T_0 and projection L_{hor}.

One should bear in mind, however, that for inclined source, the effect of horizontal directivity in Eq. (7) is about twice more pronounced than the vertical one due to the influence of the alternating sign factor $\cos(\alpha - \alpha_0)$, while p_{ver} is always nonnegative. Besides

depth phases pP, pS, sP and sS of shallow-focus earthquakes contaminate analyzed body wave records because these phases have a takeoff angle different to that of direct waves (equal to $180° - i_h$) and so they have a different direction cosine. On the other hand, the signal to noise ratio is less for body waves than for surface ones, and the range of directivity parameter for P-waves narrows owing to their higher phase velocities. Thus, we can expect that a precision of determination of the vertical directivity angle i_0 will be smaller than that of the horizontal angle α_0 and that, in general, it is better to do retrieval of the rupture direction under joint use of body and surface wave data.

It has been proved in Velasco et al. (1994b) that in the case of linear source the time function observed perpendicular to the rupture $z_\perp(t)$ is simply scaled and stretched by means of the coordinate transformation $x = V_R t$ approximation of the slip distribution $S(x)$ on the fault:

$$S(V_R t) = \frac{z_\perp(t)}{V_R \mu W}. \qquad (8)$$

Here μ is the rigidity of the material in the vicinity of the fault, W is the rupture width in the shift plane. This equation was derived on the assumption that a source dislocation is localized in time near the rupture front, so for the periods of interest the slip function reflecting the process of displacement growth at some fault point is approximately the step function. Calculated using this relationship, the slip distribution curve along the rupture of the earthquake 1992 Landers, CA ($M_W = 7.3$) coincides in shape quite well with the one measured at the surface of the causal fault but exceeds its amplitude by approximately 25% (Velasco et al., 1994b).

5. Applications of method

The model of linear source is the simplest that allows us to catch both horizontal and vertical directivity effects of the source rupture process. By way of illustration, an attempt to estimate them in a first approximation is made herein for two Russian Far East large earthquakes with opposite types of focal mechanism orientation—strike slip and dip slip. The former is

not a matter of interest in the context of the vertical directivity effect but enables us to test the method, especially in the case when a generating fault rupturing along the earth surface exposes and is well studied. In the case of near dip slip focal mechanism orientation, the strike difference of nodal planes is close to 180° and knowledge of only an azimuth of the rupture propagation will not answer the question of which of the nodal planes is the actual fault plane. Therefore, it fits the case when detection and estimation of the vertical directivity effect, if any, can resolve this ambiguity.

The dip slip (thrust) focal mechanism is typical for earthquakes that occur beneath the continental slope of the deep-sea trench of the Kuril—Kamchatka island arc. In accordance with Kikuchi and Kanamori (1995), Katsumata et al. (1995), Rogozhin and Zakharova (1998), and Rogozhin and Yunga (1999) depending on the active nodal plane orientation these earthquakes can be subdivided into two types. The first is the interplate type with a gentle active nodal plane. The continental wall of such events is thrust toward the trench, and the plane of the slip gently cutting the crust clearly corresponds to the dip of the Wadati—Benioff focal zone by its spatial position. The rupture process in sources of this type directly reflects the process of subduction of the Pacific plate. The source of the 1997 Kronotsk $M_W = 7.9$ earthquake had such an interplate type (Arefiev, 1999; Rogozhin and Yunga, 1999). The second one is the intraplate type with a steep active nodal plane. In this case, the continental slope part adjacent to the deep-sea trench is thrown up along the steeper fault plane dipped east, and the island arc side is thrown down. An example of this type of event is the 1994 Shikotan $M_W = 9.3$

earthquake (Kikuchi and Kanamori, 1995; Katsumata et al., 1995; Arefiev, 1999; Rogozhin and Yunga, 1999). It seems that the intraplate type is not a subductional mechanism, but, most probably, crossing in the lithosphere beneath the continental slope, source processes of both these types mutually cause each other (Rogozhin and Zakharova, 1998).

Giving us the way to determine active nodal planes for earthquakes with dip slip focal mechanism orientation, the discussed method allows us to classify these earthquakes to the interplate or intraplate types and reach the better understanding of tectonic processes of the region of interest.

5.1. Neftegorsk earthquake 05/27/1995 $M_w = 7.1$, $M_s = 7.6$

This earthquake occurred in the northern part of the Sakhalin Island (Table 1, Fig. 1) at the poorly studied boundary of tectonic plates (Seno et al., 1996). The rupture reached the surface and was studied in detail by International epicentral expedition (Shimamoto et al., 1996a,b). By the morphology and kinematics of its seismogenerating slip, it is consistent with the near meridian fault plain of the CMT solution (Table 1) and can be classified as a steeply dipping strike-slip reverse transform fault (Rogozhin and Yunga, 1999).

This earthquake has bright indications of radiation directivity toward the north already on the level of seismograms (Kim et al., 2000). The maximum displacement in the mainshock Love wavelet registered at the station MA2 being northward of the epicenter, nearly three times as much as that registered at the YSS station residing half as near again

Table 1
The Neftegorsk and Kamchatka earthquake source parameters

Date (mm/dd/yy)	O.T. (UTC) [hh:mm:ss]	Latitude (°N)	Longitude (°E)	Depth (km)	Strike (°)	Dip (°)	Rake (°)	M_O (dyne cm)	M_W	Author
05/27/95[a]	13:03:53[b]	52.63[b]	142.83[b]	11[b]	200, 299	63, 73	160, 29	4.3×10^{26}	7.1	S. Sipkin
				18[c]	196, 287	82, 79	169, 8	4.3×10^{26}		Harvard CMT catalog
12/18/95	02:05:58[b]	52.65[b]	142.72[b]	10[c]	14, 121	51, 71	155, 41	1.3×10^{24}	5.4	Harvard CMT catalog
					201, 298	69, 73	162, 22	1.8×10^{24}	5.5	Kim et al., 2000
03/08/99[a]	12:25:49[b]	52.06[b]	159.52[b]	21[b], 15	242, 49	28, 62	101, 84	2.6×10^{26}	6.9	Harvard CMT catalog
	12:25:46	52.13	159.32	15	230, 35	29, 62	103, 83	2.4×10^{26}	6.9	University of Michigan
03/08/99	05:40:01[b]	52.13[b]	159.48[b]	28	201, 23	32, 58	89, 91	5.2×10^{24}	5.7	Harvard CMT catalog

[a] Mainshock.
[b] USGS NEIC epicentre parameters.
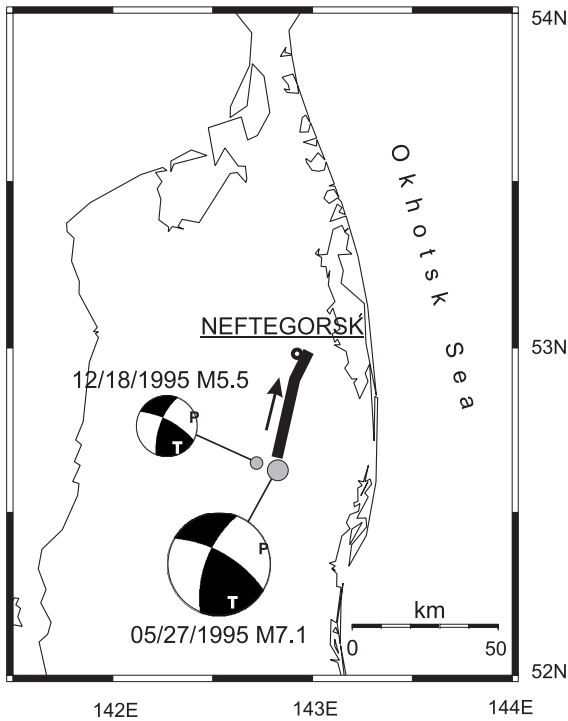[c] Source depth obtained by Sakhalin EMSD GS RAS (Fokina et al., 2001).

Fig. 1. The epicenters (gray circles) of the Neftegorsk mainshock 05/27/1995 and aftershock 12/18/1995 and their focal mechanisms (S. Sipkin solution for the mainshock (Table 1) and Kim et al. (2000) one for the aftershock). Black and open quadrants correspond to compression and dilatation. The characters P and T represent the orientation of maximum compression and tension axes, respectively. The heavy line indicates the generating fault, and the arrow shows rupture direction.

but southward. These two stations are located close to the almost meridional nodal line of this earthquake, becoming symmetrical on opposite lobes of the Love wave radiation pattern so this phenomenon cannot be explained by the focal mechanism. Besides, it is not repeated in most of the strongest aftershocks.

The 18 December 1995 aftershock ($M_W = 5.5$) is found optimal for the EGF (Fig. 1). Its magnitude is 1.6 units less than that of the main event but it was registered with a high enough S/N ratio at eight GSN stations, comparatively uniformly distributed around the epicenter (Table 2). Its focal mechanism determined by the Dreger–Langston method (Kim et al., 2000) is close to that of the mainshock. And finally, the hipocenters of this pair of events are located approximately at the same depth close to each other

(at distance 7.6 km, see source parameters in Table 1) near the south extremity of the generating fault.

Averaged over several stations and corrected for inelastic attenuation, the aftershock P-wave displacement corner frequency was found equal to $f_c^g = 0.25$ Hz. But, because the minimal resolution frequency of this aftershock records was estimated equal to $f^{S/N} = 0.16$ Hz, all deconvolved RSTFs should be additionally low pass filtered with the cutoff frequency 0.16 Hz to provide their congruency.

All deconvolved source time functions are presented in Fig. 2 in rows corresponding to the different types of waves. Fig. 3a shows how the correlation coefficient of linear regression [Eq. (5)] for durations T_R^i changes depending on the rupture dip i_0 (measured from the downwards direction) and azimuth α_0. Marked by the plus sign, the point of its maximum value $\rho_{max} = 0.95$ corresponds to the best fit to the data and indicates the rupture propagation direction: $i_0 = 85°$, $\alpha_0 = 19°$ (Table 3). Note that in the vicinity of the maximum, contours are extended along the rupture dip axis, for instance, $\rho = 0.93$ for $i_0 = 65-105°$ and $\alpha_0 = 6-34°$, so as was expected, the precision of determination of angle i_0 is less than that of angle α_0.

RSTF duration is plotted in Fig. 3c as a function of the directivity parameter computed for the rupture direction i_0, α_0 providing a maximum value of the correlation coefficient. The slope of the line is 31.5 ± 2.4 km (here and further standard error of the mean), which corresponds to the rupture length L estimation and the intercept is 19.2 ± 0.4 s, which is the actual duration of the rupture T_0.

On the other hand, the rupture parameters i_0, α_0, L of the Neftegorsk mainshock can also be estimated from the set of inverse amplitudes of deconvolved RSTFs.

Table 2
Neftegorsk earthquake data set

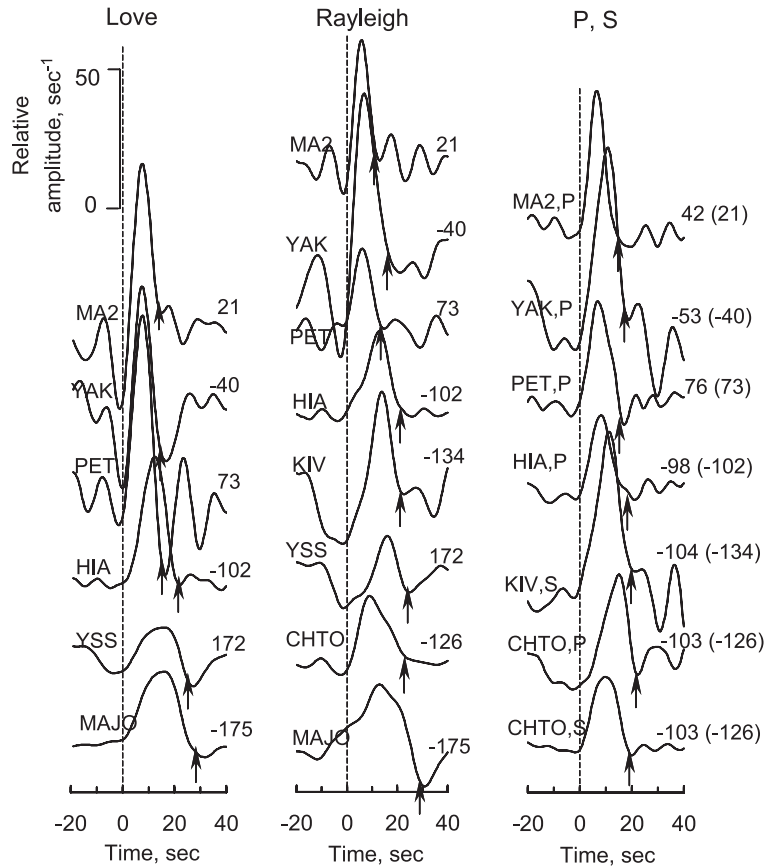| Station code	Distance (°)	Distance (km)	Azimuth (°)	Back azimuth (°)	Body wave take-off angle (°)
MA2	8.2	915	29	216	52
YAK	11.7	1304	328	137	50
PET	9.6	1062	81	266	52
HIA	14.9	1652	266	68	48
YSS	5.7	630	180	0	53
MAJO	16.4	1825	193	10	47
CHTO	47.9	5326	242	35	25
KIV	61.7	6855	234	43	22

Fig. 2. The deconvolved relative source time functions of the Neftegorsk earthquake, lined up with their onsets at zero moment of time. Arrows point to the moments interpreted as the ends of impulses. The station code and type of wavelet (P or S) in the case of body waves are indicated on the left-hand side of each cover; angle θ (°) between the obtained rupture direction and the ray leaving the source into the point of observation is indicated on the right. The difference (°) between azimuths of the rupture direction and direction to the station is shown parenthetically.

Owing to the facts that the area under the RSTF is equal to the mainshock seismic moment normalized to the auxiliary shock moment and the forms of STF pulses of the Neftegorsk mainshock (Fig. 2) are close to triangular (i.e., $AT_R \approx A_0T_0 \approx 2M/M_g$, where A and A_0 are the pulse amplitudes of RSTF and true STF, M_0 and M_g are the main and auxiliary event seismic moments), then division of Eq. (5) by AT_R gives the approximate equation for amplitudes:

$$1/A \cong 1/A_0 - L \cdot \Gamma(A_0T_0) \tag{9}$$

Results of correlation analysis of inverse amplitudes are shown on the Fig. 3b and in Table 3. The position and form of contours are close to those of durations in Fig. 3a, with the small shift along the rupture azimuth axis. RSTF's inverse amplitude is plotted in Fig. 3d as a function of the directivity parameter best fitting to the data. The slope of the line gives $L = 39.4 \pm 9.4$ km.

Taking the average from both duration and inverse amplitudes' data estimations, we see that destruction in the source propagated roughly horizontally ($\bar{i}_0 = 89 \pm 4°$) in the direction $\alpha_0 = 8 \pm 11°$ along the rupture $\bar{L} = 35.5 \pm 4.9$ km in length at the speed of $\bar{V}_R = 1.9 \pm 0.2$ km/s during $T_0 = 19.2 \pm 0.4$ s. The calculated rupture azimuth and length turned out to be close within the error to the generating fault trend N15° E and length 35 km measured by geologists (Shimamoto et al., 1996a,b).
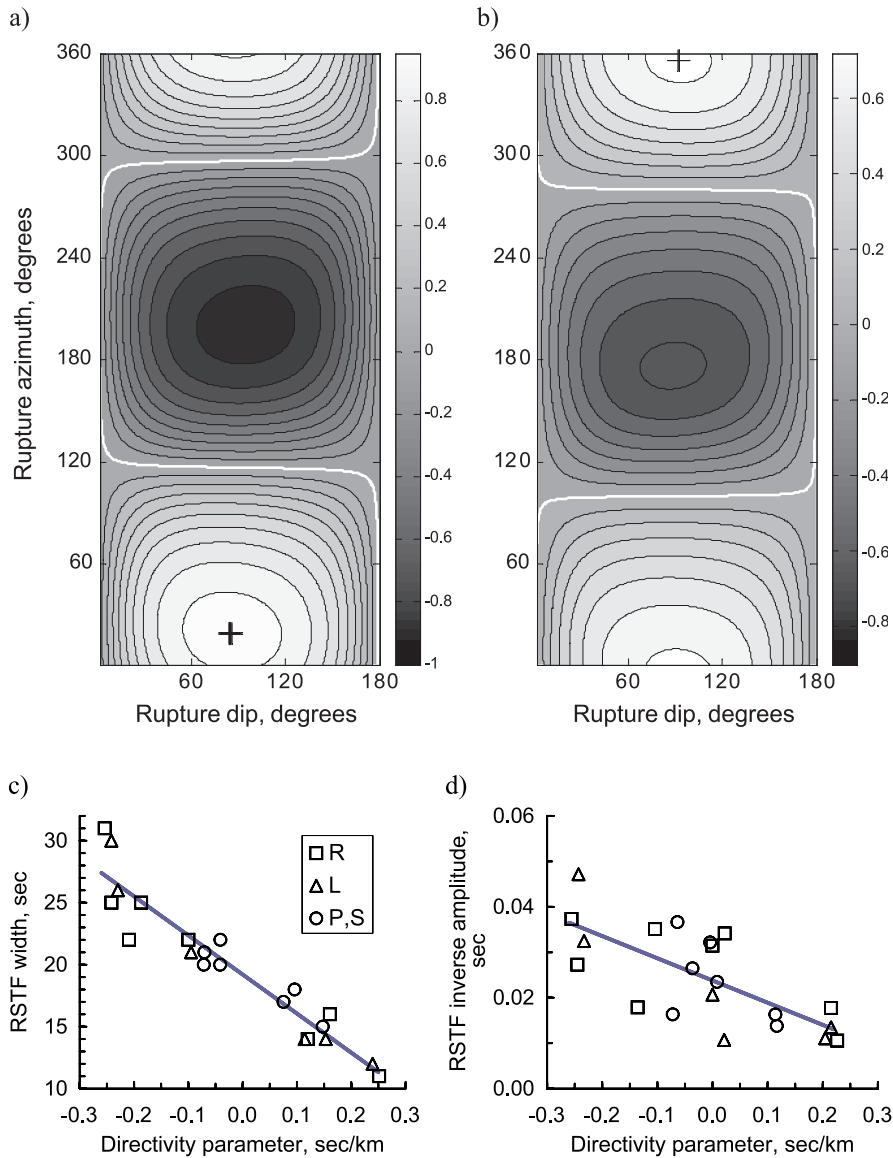
a)

b)

c)

d)

Fig. 3. The Neftegorsk earthquake directivity analysis. Variation of the correlation coefficient of linear regression [Eq. (5)] for durations (a) and of linear regression [Eq. (9)] for inverse amplitudes (b) as a function of the rupture dip i_0 and azimuth α_0. The point of the maximum value of the correlation coefficient is marked by the plus sign, contours of the correlation coefficient are drawn with the step 0.1, and the zero contour is white colored. Durations (c) and inverse amplitudes (d), normalized to the aftershock seismic moment, of retrieved relative source time functions vs. the directivity parameter calculated for the rupture direction corresponding to the maximum value of the correlation coefficient (Table 3). R, L, P and S denote those estimated from Rayleigh, Love and body waves, respectively. The solid line indicates the best fitting line.

The directivity analysis was also carried out for times of peaks T_R^{max} of the deconvolved pulses. Its results presented in Table 3 show that the maximum moment release occurred actually in the same direction as the entire rupture at a distance of 16.9 ± 2.2 km from the epicenter and 9.7 ± 0.4 s after the rupture process started.

The station HIA in China is located under the angle $-102 \pm 11°$ or nearly perpendicular to the calculated rupture propagation direction, so its directivity effect is

Table 3
Results of the directivity analysis of RSTF durations (T_R), locations of their peaks (T_R^{max}) and inverse amplitudes ($1/A$)

Number of RSTFs	Kind of data	ρ_{max}	i_0	α_0	T_0 (s) A_0 (s^{-1})	$\pm\sigma_{T_0}$ (s) $\pm\sigma_{A_0}$ (s^{-1})	L (km)	$\pm\sigma_L$ (km)
Neftegorsk earthquake								
21	T_R	0.95	85	19	19.2	0.4	31.5	2.4
21	$T^{max}{}_R$	0.87	85	16	9.7	0.4	16.9	2.2
21	$1/A$	0.72	92	356	42.0	3.0	39.4	9.4
Kamchatka earthquake								
39	T_R	0.87	30	156	13.4	0.2	25.5	2.3
39	$1/A$	0.24	60	164	6.4	0.1	1.4	1.0

minimal. On the average RSTF deconvolved (without additional filtration for congruency of all STFs) from Love and Rayleigh waves registered at this station, the static displacement distribution curve along the fault was calculated in accordance with Eq. (8). It was assumed that $M_g = 1.3 \times 10^{24}$ dyne·cm (Harvard CMT estimation), and $W = 13$ km (Arefiev and Dorbat, 2001). The value of rigidity was estimated on the assumption of equal Lame constants from the formula

$$\mu = \rho V_P^2/3, \tag{10}$$

where density ρ was determined from P-wave velocity V_P using the equation (Berteussen, 1977)

$$\rho = 0.32 V_P + 0.77 \tag{11}$$

Thus we have that for $V_P = 5.6$ km/s (Arefiev and Dorbat, 2001), $\rho = 2.56$ g/cm^3 and $\mu = 2.7 \times 10^{11}$ dyne/cm^2. Then for found from Eq. (9) $A_0 = 42.0 \pm 3.0$ s^{-1} (Table 3), the maximum slip on the fault is $S_{max} = 8.4 \pm 1.3$ m. The average slip on the fault calculated by the formula of the seismic moment

$$M_0 = \mu W L \bar{U}, \tag{12}$$

is then $\bar{U} = 3.5 \pm 0.5$ m for $M_0 = 4.3 \times 10^{26}$ dyne·cm (Table 1). Direct measurements on the exposed generating fault surface gave almost the same estimations of maximum and average slip: $S_{max} = 8.1$ m and $\bar{U} = 3.8$ m (Shimamoto et al., 1996a).

The computed slip distribution along the rupture is shown in Fig. 4 (curve 1) together with the results of the observed horizontal offset measurements made by geologists (curve 2). As would be expected, the calculated curve is smoothed compared with the experimen-

tal one but repeats the main particularities of its form; the small offset peak at $5–8$ km from the epicenter and the main maximum at approximately 21 km from the onset of rupture. Thus, we can see at least two asperities or subevents. Note that the first small asperity is clearly distinguishable only on the three RSTFs registered at HIA, KIV and YSS (Fig. 2). Also characteristically, that the slip value quickly declines on the last 10 km of this rupture (in the direction from south to north).

The fact of close agreement between the predicted and real fault parameters proves that the source of the Neftegorsk earthquake is well described by the model of the linear unilateral fault, and contradicts the new complex bilateral source model with a total rupture length of 46 km proposed in Arefiev (1999) and Arefiev et al. (2000).

5.2. Kamchatka earthquake 03/08/1999 $M_w = 6.9$, $M_s = 7.1$

This event occurred near the eastern seacoast of Kamchatka in the Avacha bay and is rather representative for this region. Its source was located beneath the continental slope of the deep-sea trench of the Kuril–Kamchatka island arc (Table 1, Fig. 5). The first foreshock with magnitude $M_W = 5.8$, which is more than one unit less than that of the mainshock, is acceptable for the EGF. It happened 6 h before the mainshock, at a distance of $8–11$ and $7–13$ km
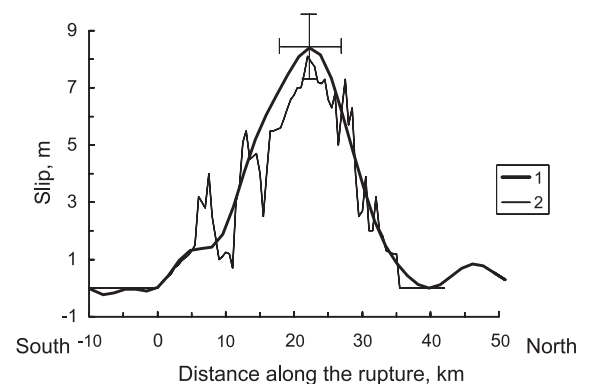

Fig. 4. Fault slip distribution for the Neftegorsk earthquake, which is the average of Love and Rayleigh RSTFs deconvolved at HIA (line 1) and that (line 2) observed on the surface rupture (Shimamoto et al., 1996a,b). In the point of maximum, the root mean square errors of the estimated maximum slip amplitude (± 1.3 m) and rupture length (± 4.9 km) are shown.
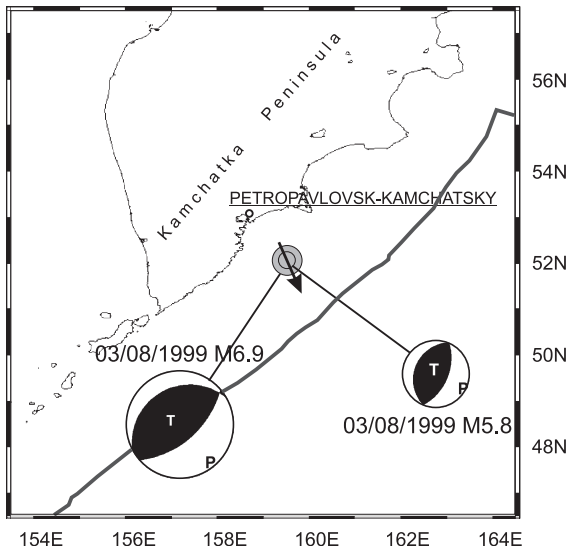
Fig. 5. The epicenters (gray circles) of the Kamchatka earthquake 03/08/1999 and its first foreshock and their focal mechanisms (Harvard CMT catalog). Black and open quadrants correspond to compression and dilatation. The characters P and T represent the orientation of maximum compression and tension axes, respectively. The arrow shows rupture direction. The position of the Kuril–Kamchatka deep-sea trench axis is shown by thick black line.

beneath it (Table 1), and was registered with a small enough noise level at 13 GSN stations (Table 4). The focal mechanism of this pair of events is nearly pure upthrust. Being almost similar, their mechanism solutions are turned by $29-41°$ and $12-26°$ in strike of their nodal planes (Table 1). The first nodal plane is slightly inclined to the Kamchatka peninsula, and the second is steeply fallen to the ocean.

It should be noticed also that in the case of rupture propagation oblique to horizon, the range of values of the directivity parameter is narrowing. Besides, because in the given case all stations are posed in the west sector relative to the near vertical fault plane, this already truncated range is contracted again. These circumstances are serious testing agents of the method resolution.

The foreshock P wave corner frequency after correction for inelastic attenuation was estimated as $f_c^g = 0.24$ Hz, the minimal resolution frequency as $f^{S/N} = 0.17$ Hz. Therefore, before the directivity analysis, all RSTFs deconvolved at different stations were low pass filtered with the cutoff frequency 0.17 Hz for ensuring their congruency.

All RSTFs deconvolved from Love, Rayleigh and P-waves are shown in Fig. 6. The noticeable variation of RSTF duration with azimuth tells us about the possible existence of the rupture directivity effect. Fig. 7a shows how the correlation coefficient of linear regression [Eq. (5)] for durations T_R^i of the deconvolved RSTFs changes depending on a rupture dip i_0 (measured from the downwards direction) and azimuth α_0. The point of maximum correlation coefficient $\rho_{max} = 0.87$ indicates the rupture propagation direction: angle with horizon $i_0 = 30°$ and azimuth $\alpha_0 = 156°$ (Table 3). Note that forms of contours of equal values of the correlation coefficient are essentially different from those for the Neftegorsk mainshock, but as before, the close to maximum correlation coefficient gives the range of the rupture dip half as large again as that of the rupture azimuth ($\rho = 0.85$ for $i_0 = 14-53°$ and $\alpha_0 = 144-170°$), so the precision of determination of angle i_0 is less than that of angle α_0. The estimations made for the found rupture direction are the following: rupture length $L = 25.5 \pm 2.3$ km, duration $T_0 = 13.4 \pm 0.2$ s (Table 3, Fig. 7c) and average rupture velocity $V_R = 1.9 \pm 0.2$ km/s.

Besides the noticeable variation in RSTF duration with azimuth in Fig. 6, we can see that the position of the main peak of the pulses corresponding to the maximum moment release almost does not change and its time relative to the onset with few exceptions is $4-5$ s. It can be understood that the early process of the moment release growth to maximum was quick

Table 4
Kamchatka earthquake data set

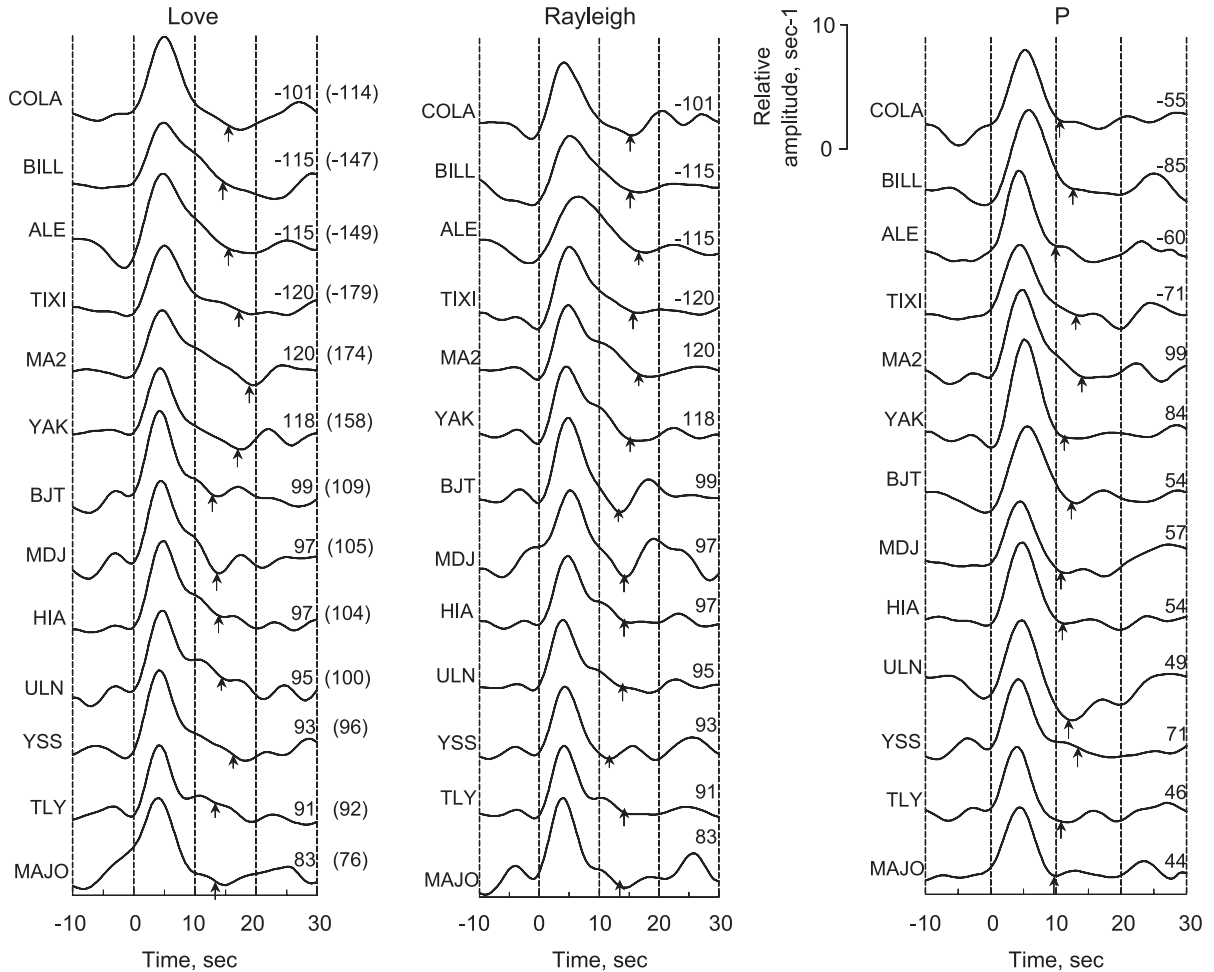| Station code	Distance (°)	Distance (km)	Azimuth (°)	Back azimuth (°)	Body wave take-off angle (°)
COLA	29.3	3252	44	270	37
BILL	16.4	1818	9	195	59
ALE	43.8	4866	7	324	32
TIXI	23.8	2644	337	129	41
MA2	9.0	997	330	143	69
YAK	18.8	2090	314	108	56
BJT	31.9	3540	265	53	37
MDJ	21.1	2341	261	58	43
HIA	25.1	2785	260	68	40
ULN	33.3	3699	256	63	36
YSS	12.0	1332	252	59	65
TLY	33.7	3739	248	67	36
MAJO	21.6	2402	232	37	43

Fig. 6. The retrieved relative source time functions of the Kamchatka earthquake, lined up with their onsets at zero moment of time. Arrows point to the moments interpreted as the ends of impulses. The station code is indicated on the left-hand side of each cover; angle θ (°) between the obtained rupture direction and the ray leaving the source into the point of observation is indicated on the right. The difference (°) between azimuths of the rupture direction and direction to the station is shown parenthetically.

(4–5 s) and not directed (bilateral within the scope of the linear source model). To prove this presumption, one can do the directivity analysis of inverse amplitudes, the results of which in the case of this earthquake will not concern the process as a whole but only its early stage.

Correlation analysis of the inverse amplitudes set (Fig. 7b) gives a very small value of the maximum correlation: $\rho_{max} = 0.24$ at $i_0 = 60°$ and $\alpha_0 = 164°$ (Table 3), but the position and form of contours are surprisingly close to those of durations in Fig. 7a. This means that the early process of the moment

release growth was indeed hardly directed, with the very small component of overall propagation in the same direction as the whole process. Its estimation from the slope of the best fitting line (Fig. 7d) gives $L = 1.4 \pm 1.0$ km (Table 3) for $T_0 \approx 4.5$ s (the time of the main maximum moment release).

Estimating further $W \approx L/2 = 12.7$ km and $V_P = 6.6$ km/s (Gorbatov et al., 1999), for $A_0 = 6.4 \pm 0.1$ s^{-1} (Table 3) and $M_g = 5.2 \times 10^{24}$ dyne·cm (Table 1) it can be determined from Eqs. (8), (10)–(12) the maximum and average slip on the fault $S_{max} = 3.3 \pm 0.5$ m and $\bar{U} = 1.9 \pm 0.2$ m (for $M_0 = 2.6 \times 10^{26}$ dyne·cm,
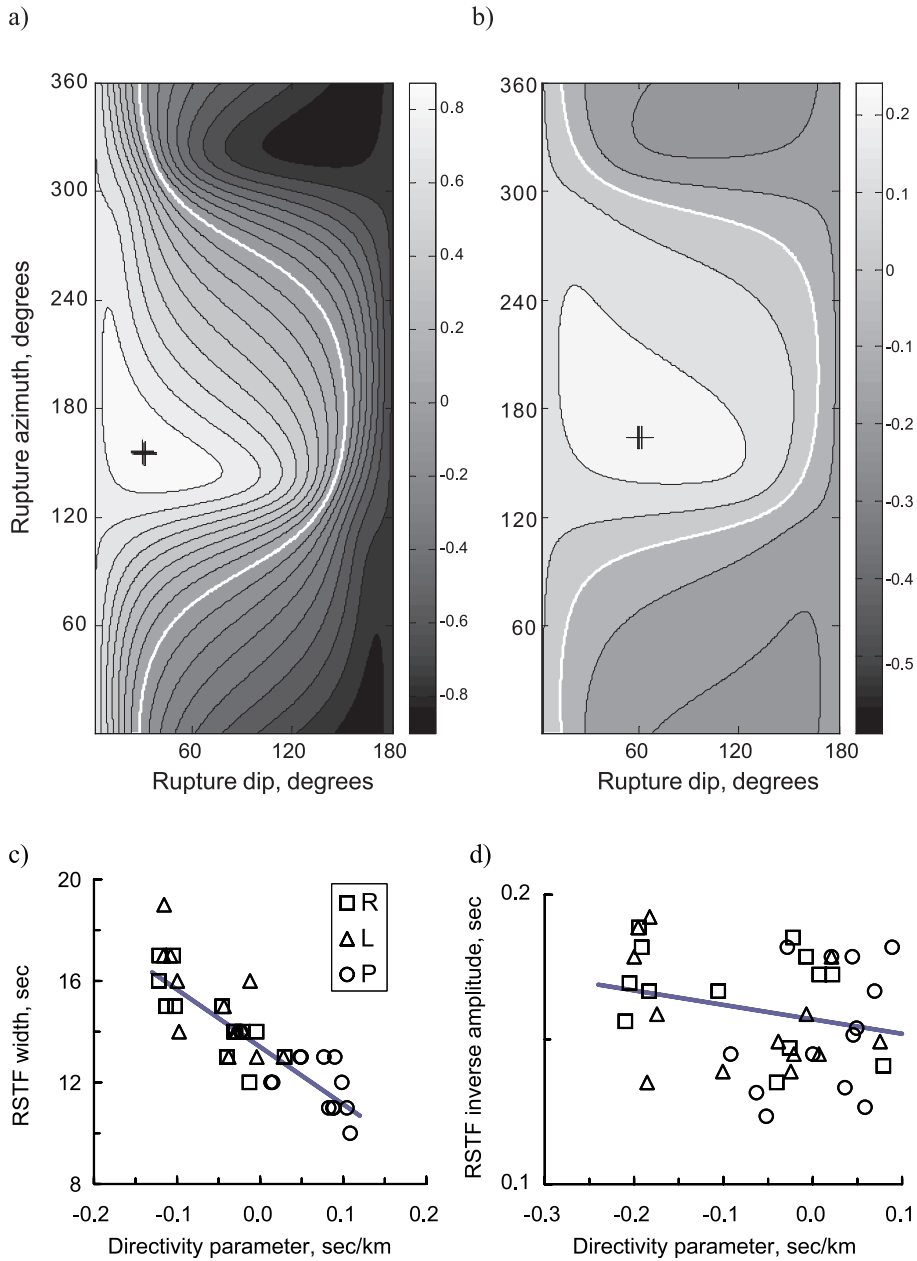
a)

b)

c)

d)

Fig. 7. The Kamchatka earthquake directivity analysis. Variation of the correlation coefficient of linear regression [Eq. (5)] for durations (a) and of linear regression [Eq. (9)] for inverse amplitudes (b) as a function of the rupture dip i_0 and azimuth α_0. The point of the maximum value of the correlation coefficient is marked by the plus sign, contours of the correlation coefficient are drawn with the step 0.1, and the zero contour is white colored. Durations (c) and inverse amplitudes (d), normalized to the foreshock seismic moment, of retrieved relative source time functions vs. the directivity parameter calculated for the rupture direction corresponding to the maximum value of the correlation coefficient (Table 3). R, L and P denote those estimated from Rayleigh, Love and body waves P, respectively. The solid line indicates the best fitting line.
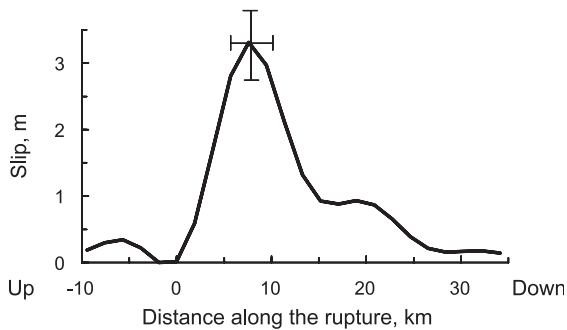
Fig. 8. Fault slip distribution for the Kamchatska earthquake, which is the average of Love and Rayleigh RSTFs deconvolved at TLY. In the point of maximum, the root mean square errors of the estimated maximum slip amplitude (± 0.5 m) and rupture length (± 2.3 km) are shown.

Table 1). The average of the Love and Rayleigh wave RSTFs calculated for station TLY was used to generate the slip distribution (Fig. 8). It shows that the Kamchatka earthquake mainshock source consisted roughly of two subevents; the first with the maximum slip 3.3 m at approximately 7 km from the onset of rupture, and the second with the maximum slip about 0.9 m centered at about 19 km from that. Unfortunately, the second asperity is seen only on some RSTFs and the positions and magnitudes of its maximum cannot be estimated exactly to apply the directivity analysis and study details of the rupture process separately.

To sum up, it may be said that the overall rupture direction vector, found for the Kamchatka earthquake, belongs to the steeply fallen to the ocean fault plane, so this earthquake can be referred to the intraplate type. The destruction in the source propagated from top to bottom, resulting in the continental (Kamchatka) wall being thrown down relative to the continental slope part adjacent to the deep-sea trench. Thus, starting at a depth of about 10–20 km within the Eurasian plate, the rupture process propagated towards the upper surface of the Pacific subducted slab located in the region of this earthquake at a depth of 45–50 km (Gorbatov et al., 1999).

6. Conclusions

Based on the model of the linear unilateral fault, it is shown that the source finiteness has the horizontal

and vertical components and the effect of vertical directivity can be detected only from body wave data. However, owing to its lesser accuracy than that of surface waves, it will be good practice to carry out the directivity analysis incorporating both kinds of data. Detection of the vertical directivity is particularly useful for the choice of active nodal planes of earthquakes with the dip slip fault orientation that allows us to classify these earthquakes to the interplate or intraplate types and reach the better understanding of tectonic processes in the region of interest.

Tikhonov's technique, using input errors for the parameter of regularization calculation, gives a real and stable estimation of deconvolved source functions. The reliable determination of their amplitudes allows us not only to get ultimately the reliable estimation of a slip distribution along the fault but also include them into the directivity analysis. A way to do all restored RSTFs comparable with each other on the smoothing degree to provide their congruency at the directivity analysis and to improve its accuracy has been presented here.

As a result of application of the method to the 1995 Neftegorsk and 1999 Kamchatka earthquakes, the average parameters of their faulting process were estimated including the fault orientation in space, rupture length, duration, velocity and slip distribution along the fault. As for the Neftegorsk earthquake, we see close agreement between the predicted and real fault parameters that proves that its source is well described by the model of the linear unilateral fault and gives a good assessment of the method applied. The overall rupture direction vector, found for the Kamchatka earthquake, belongs to the steeply fallen to the ocean fault plane. Hence, it appears that the destruction propagated from top to bottom, resulting in the continental (Kamchatka) wall being thrown down relative to the continental slope part adjacent to the deep-sea trench. Therefore, this event can be regarded as intraplate type.

Yanovskaya and Dr. A. Ivaschcenko, for their help and encouragement; and the researchers of the St. Petersburg State University and IMGG for their attention and helpful discussions. I thank the anonymous reviewer and Dr. Y. Tanioka for their constructive suggestions to improve the manuscript.

References

Ammon, C.J., Velasco, A.A., Lay, T., 1993. Rapid estimation of rupture directivity: application to the 1992 Landers ($M_S = 7.4$) and Cape Mendocino ($M_S = 7.2$), California earthquakes. Geophys. Res. Lett. 20, 97–100.

Arefiev, S.S., 1999. The strongest earthquakes that occurred in the territory of Russia in recent years. National report (1995–1998) of National Geophys. Comm. of Russian Acad. Sc. to IASPEI, Intern. Un. Geod. Geophys., Moscow, http://www.wdcb.ru/NGC/.

Arefiev, S.S., Dorbat, C., 2001. The 1995 Neftegorsk earthquake: tomography of the source zone. Izv.-Russ. Acad. Sci., Phys. Solid Earth 37 (2), 141–150.

Arefiev, S., Rogozhin, E., Tatevossian, R., Rivera, L., Cisternas, A., 2000. The Neftegorsk (Sakhalin island) 1995 earthquake: a rare interplate event. Geophys. J. Int. 143, 595–607.

Beck, S.L., Ruff, L.J., 1984. The rupture process of the great 1979 Columbia earthquake: evidence for the asperity model. J. Geophys. Res. 89, 9281–9291.

Berteussen, K.A., 1977. Moho depth determination based on spectral ratio analyze of NORSAR long-period P-wave. Phys. Earth Planet. Inter. 15, 13–27.

Cassidy, J.F., 1995. Rupture directivity and slip distribution for the M_S 6.8 earthquake of 6 April 1992, offshore British Columbia: an application of the empirical Green's function method using surface waves. Bull. Seismol. Soc. Am. 85, 736–746.

Fokina, T.A., Poplavskaya, L.N., Sholokhova, A.A., Sadchikova, A.A., Velichko, L.F., Parshina, I.A., Levit, E.V., 2001. Sakhalin (catalog of earthquakes). Zemletryasenia Severnoi Evrazii v 1995 (Earthquakes in Eurasia in 1995. Journal of Earthquake Prediction Research). GSRAS, Moscow, pp. 311–322. (in Russian).

Gorbatov, A., Dominguez, J., Suarez, G., Kostoglodov, V., Zhao, D., Gordeev, E., 1999. Tomographic imaging of the P-wave velocity structure beneath the Kamchatka peninsula. Geophys. J. Int. 137, 269–279.

Gurrola, H., Baker, G.E., Minster, J.B., 1995. Simultaneous time-domain deconvolution with application to the computation of receiver functions. Geophys. J. Int. 120, 537–543.

Hartzell, S.H., 1978. Earthquake aftershocks as Green's functions. Geophys. Res. Lett. 5, 1–5.

Haskell, N.A., 1964. Total energy and energy spectral density of elastic wave radiation from propagating faults. Bull. Seismol. Soc. Am. 54, 1811–1841.

Hough, S.E., Dreger, D.S., 1995. Source parameters of the 23 April 1992 M 6.1 Joshua Tree, California, earthquake and its after-shocks: empirical Green's function analysis of GEOS and TER-RAscope data. Bull. Seismol. Soc. Am. 85, 1576–1590.

Katsumata, K., Ichiyanadi, M., Miwa, M., Kasahara, M., 1995. Aftershock distribution of the October 4, 1994 M_w 8.3 Kuril Island earthquake determined by a local seismic network in Hokkaido, Japan. Geophys. Res. Lett. 22, 1321–1324.

Kikuchi, M., Kanamori, H., 1995. The Shikotan earthquake of October 4, 1994: litospheric earthquake. Geophys. Res. Lett. 22, 1025–1028.

Kim, S.G., Kraeva, N., Chen, Y.T., 2000. Source parameter determination of regional earthquakes in the Far East using moment tensor inversion of single-station data. Tectonophysics 317, 125–136.

Kraeva, N.V., 1996. Shallow-focus earthquakes in the South Sakhalin recorded by IRIS-2 system 1993–1995. Bull. Seism. Assoc. Far East 2 (1), 64–72.

Kraeva, N.V., 2001. Average parameters of the source rupture process of crust earthquakes estimation. PhD thesis. St. Petersburg State University, St-Petersburg. (in Russian).

Kraeva, N.V., 2003. Estimation of average parameters of faulting in crust earthquakes. XXIII General Assembly of the International Union of Geodesy and Geophysics IUGG2003 (June 30–July 11, 2003), Sapporo, Japan. Abstracts (Theses). JaMSTeC, Japan, A.451.

Lay, T., Wallace, T., 1995. Modern global seismology. International Geophysics Series. Academic, USA, p. 58.

Li, Y., Thurber, C.H., 1988. Source properties of two microearthquakes at Kilauea Volcano Hawaii. Bull. Seismol. Soc. Am. 78, 1123–1132.

Mori, J., 1996. Rupture directivity and slip distribution of the M 4.3 foreshock to the 1992 Joshua Tree earthquake, Southern California. Bull. Seismol. Soc. Am. 86, 805–810.

Mori, J., Frankel, A., 1990. Source parameters for small events associated with the 1986 North Palm Springs, California, earthquake determined using empirical Green functions. Bull. Seismol. Soc. Am. 80, 278–295.

Mueller, C., 1985. Source pulse enhancement by deconvolution of an empirical Green's function. Geophys. Res. Lett. 12, 33–36.

Owens, T.J., Zandt, G., Taylor, S.R., 1984. Seismic evidence for an ancient rift beneath the Cumberland Plateau, Tennessee: a detailed analysis of broadband teleseismic P waveforms. J. Geophys. Res. 89 (B9), 7783–7795.

Rogozhin, E.A., Yunga, S.L., 1999. Seismotectonics of largest earthquakes in Northern Eurasia at the end of 20 century based on seismological IRIS data. Bull. Russ. Acad. Sci. Geol. Geophys. Geochem. Mining Sc. Section 1, 14–29.

Rogozhin, E.A., Zakharova, A.I., 1998. The tectonic nature of the seismic activation 1994–1996 at the east active outskirt of Asia. Tektonika i geodinamika: obshcie i regionalnye aspekty (Tectonics and Geodynamics: General and Regional Aspects). Proc. of the XXXI Tectonic Conference, Russ. Ac. Sc., Geol. Geophys. Geochem. Mining Sc. Section, 27–30 January 1998, Moscow, vol. 2. Geos, pp. 118–121. (in Russian).

Ruff, L., Kanamori, H., 1983. The rupture process and asperity distribution of three great earthquakes from long-period diffracted P-waves. Phys. Earth Planet. Inter. 31, 201–230.

Schwartz, S.Y., Ruff, L.J., 1985. The 1968 Tokachi-Oki and the 1969 Kurile Islands earthquakes: variability in the rupture process. J. Geopys. Res. 90, 8613–8626.

Seno, T., Sakurai, T., Stein, S., 1996. Can the Okhotsk plate be discriminated from the North American plate? J. Geophys. Res. 101, 11305–11315.

Sherbaum, F., 1996. Of poles and zeros: fundamentals of digital seismology. Modern Approach in Geophysics vol. 15. Kluwer Academic Publishing, Dordrecht.

Sherbaum, F., Johnson, J., 1994. Programmable interactive toolbox for seismological analysis (PITSA). IASPEI Software Library 5, Student edition. Serito, CA, USA.

Shimamoto, T., Watanabe, M., Suzuki, Y., 1996a. Surface faults associated with the 1995 Neftegorsk earthquake. The Island Arc 7, 203–220.

Shimamoto, T., Watanabe, M., Suzuki, Y., Kozhurin, A.I., Strel'tsov, M.I., Rogozhin, E., 1996b. Surface faults and damage associated with the 1995 Neftegorsk earthquake. J. Geol. Soc. Jpn. 102, 894–907.

Sipkin, S.A., Lerner-Lam, A.L., 1992. Pulse-shape distortion introduced by broadband deconvolution. Bull. Seismol. Soc. Am. 82, 238–258.

Tikhonov, A., Arsenin, V., 1977. Solutions of Ill-Posed Problems Winston and Sons, Washington, DC.

Tikhonov, A.N., Glasko, V.B., Kriksin, Yu.A., 1979. On the question about quasioptimal choice of the regularized approximation. Doclady AN SSSR (Reports of Academy of Sciences of USSR) 248 (3), 531–535 (in Russian).

Tikhonov, A.N., Goncharskiy, A.V., Stepanov, V.V., Yagola, A.G., 1995. Numerical Methods for the Solution of Ill-Posed Problems. Kluwer Academic Publishing, Dordrecht.

Velasco, A., Ammon, J., Lay, T., 1994a. Recent large earthquakes near Cape Mendocino and in the Gorda Plate: broadband source time functions, fault orientations and rupture complexities. J. Geophys. Res. 99, 711–728.

Velasco, A., Ammon, J., Lay, T., 1994b. Empirical Green function deconvolution of broadband surface waves: rupture directivity of the 1992 Landers, California ($M_w = 7.3$), earthquake. Bull. Seismol. Soc. Am. 84, 735–750.

Zollo, A., Capuano, P., Singh, S.K., 1995. Use of small earthquake records to determine the source time functions of larger earthquakes: an alternative method and an application. Bull. Seismol. Soc. Am. 85, 1249–1256.